analytical chemistry

Article

pubs.acs.org/ac

Label-Free Single Cell Kinetics of the Invasion of Spheroidal Colon Cancer Cells through 3D Matrigel

Nicole K. Febles,[†] Ann M. Ferrie, and Ye Fang*

Biochemical Technologies, Science and Technology Division, Corning Incorporated, Corning, New York 14831, United States

ABSTRACT: This article reports label-free, real-time, and single-cell quantification of the invasion of spheroidal colon cancer cells through three-dimensional (3D) Matrigel using a resonant waveguide grating (RWG) imager. This imager employs a time-resolved swept wavelength interrogation scheme to monitor cell invasion and adhesion with a temporal resolution up to 3 s and a spatial resolution of 12 μm. As the model system, spheroids of human colorectal adenocarcinoma HT-29 cells are generated by culturing the cells in 96-well round-bottom ultralow attachment plates. 3D Matrigel is formed by its gelation in 384-well RWG biosensor microplates. The invasion and adhesion of spheroidal HT29 cells is initiated by placing individual spheroids onto the Matrigel-coated biosensors. The time series RWG images are obtained and used to extract the optical signatures arising from the adhesion after the cells are dissociated from the spheroids and invade through the 3D Matrigel. Compound profiling shows that epidermal growth factor accelerates cancer cell invasion, while vandetanib, a multitarget kinase inhibitor, dose-dependently inhibits invasion. This study demonstrates that the label-free imager can monitor in real-time the invasion of spheroidal cancer cells through 3D matrices.

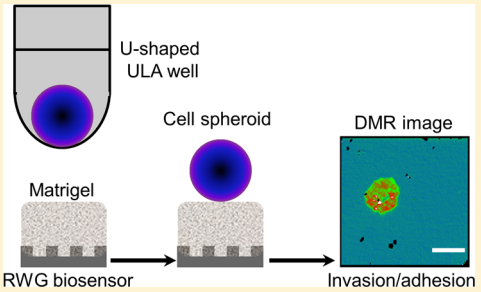

Tumor invasion and metastasis is a multistep cascade process consisting of local invasion of cancer cells through the extracellular matrix (ECM) and stromal cell layers, then intravasation into the lumina of blood vessels, transit through the lymphatic and hematogenous systems, arrest and extravasation out of the circulatory system, and the formation and growth of micrometastatic lesions into macroscopic tumors at a distant site.[1−3] Tumor cells utilize diverse mechanisms including individual and collective cell migration strategies to infiltrate their primary tissue and metastasize to distant sites.[4−6] Local invasion of tumor cells through the ECM or basement membrane is a complex process involving adhesion, proteolytic remodeling of the ECM, and migration.[7,8] The basement membrane is a thin ECM that underlies and separates epithelia/endothelia from the stroma. Tumor cells produce proteases to degrade the membrane so they can cross the membrane, invade the stroma, and establish distant metastases. Tumor invasion and metastasis is the main cause of cancer-associated patient mortality; inhibitors targeting these processes represent promising opportunities for developing anticancer targeted therapeutics.[9,10]

In vitro invasion assays, in particular those mimicking the in vivo process, are useful for elucidating the mechanisms by which tumor cells acquire an invasive phenotype and also for discovering new targeted therapeutics.[11−14] The most common in vitro invasion assay, the Transwell assay, employs a modified Boyden chamber, in which Matrigel is used to coat the porous membrane separating the upper and lower chambers, and cells are seeded on top in the upper chamber.[12] Single cells that have invaded to the underside of the chamber are counted to determine their invasive potential. Introducing a chemo-attractant in the lower chamber further enables chemotaxis analysis. As a gelatinous protein mixture secreted by Engelbreth−Holm−Swarm (EHS) mouse sarcoma cells, Matrigel is the most widely used basement membrane because of its reliability and reproducibility, and consists mainly of laminin-111, collagen IV, heparan sulfate proteoglycan, various growth factors, proteases, and additional components.[15,16] However, this assay only permits an end point measurement by counting the number of invaded cells. In addition, this assay has limited ability to recapitulate in vivo process, as tumors often display vast structural heterogeneity and invade in three dimensions, often as multicellular clusters.[17] To address these limitations new assays have been developed.[18−24] However, these assays mostly rely on imaging techniques to track the shape and location of cells in a three-dimensional (3D) matrix, and often examine invasion of individual cells in suspension.

3D multicellular spheroids have been postulated to span the gap between two-dimensional (2D) culture models and whole-animal systems.[25,26] 2D monolayer cell culture models, although long used for basic research and drug screening, simply do not reflect the multicellular microenvironments found in the body and have proven to be a relatively poor drug development model for anticancer drug discovery.[27,28] Compared to 2D, in vitro 3D multicellular spheroids more closely recapitulate the in vivo situation of solid cancers and may help to accelerate translational research in cancer biology, as these 3D models have better predictive power for cancer cell growth,[29] invasive potential,[30] and drug responsiveness,[31,32] as well as mimic better phenotypic heterogeneity[33,34] and

Received: June 20, 2014
Accepted: August 13, 2014
Published: August 13, 2014

   dx.doi.org/10.1021/ac502269v | *Anal. Chem.* 2014, 86, 8842−8849

microenvironments of tumors.[35] Recently, several in vitro assays have been developed to investigate the invasion of single cells in suspension[36,37] or a spheroidal structure[38,39] of a first cell type into the spheroidal cluster of a second cell type. However, these assays often use fluorescently labeled cells and have low temporal resolution. The quantification of invading cells is also cumbersome, because these assays often requires deep confocal imaging, flow cytometry after trypsinization, or immunohistochemistry after paraffin embedding and tissue sectioning, all of which imply special equipment and extensive pre- and postexperimental processing.[24] The invasion of spheroidal cell clusters through 3D ECM gel has also been studied using light microscopy in real time.[40,41] However, light microscopic imaging is limited to visualize the outer border of spheroids placed in the gel, so only invasion events at late stages can be examined. Therefore, an assay that enables real-time, single-cell, and quantitative monitoring of the invasion of spheroidal cells through a 3D matrix would be great advantageous.

Herein, we report a resonant waveguide grating (RWG) biosensor-based spheroidal cancer cell invasion assay. This assay consists of three critical steps (Figure 1). First, 3D Matrigel film is formed on the biosensor surface through gelation of Matrigel at 37 °C overnight. Second, spheroids of human colorectal adenocarcinoma HT29 cells are generated through culturing cells in Corning ultra-low attachment (ULA) 96-well plates, and used as the model system. Third, a spatially resolved RWG imager[42,43] is used to monitor and quantify the dynamic mass redistribution (DMR) signals arising from the adhesion after the cells are dissociated from the spheroidal structure and invade through the Matrigel. The DMR signal is recorded as the shift in resonant wavelength in picometer (pm). The RWG biosensor is a label-free optical biosensor centered on waveguide nanograting arrays embedded in standard microtiter plates,[44] enabling real-time whole cell sensing, in particular for receptor signaling[45−49] and drug pharmacology assessment.[50−55] Taking advantage of the relatively short sensing depth (~150 nm) of the biosensors[44] as well as the high spatial resolution of the imager, we demonstrated that this system offers a label-free, real-time, single cell and quantitative means to study the invasion process of cancer cells in spheroids through 3D ECM gels.

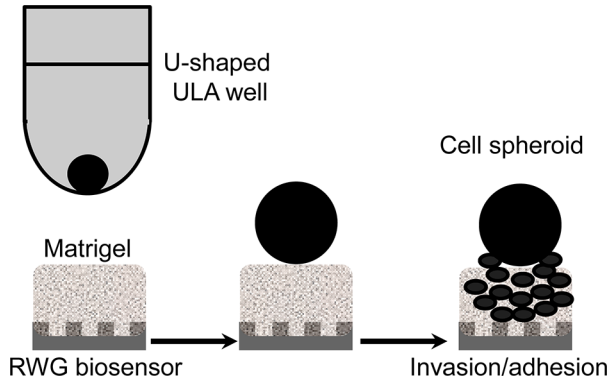

Figure 1. Schematic of a label-free resonant waveguide grating (RWG) biosensor-based invasion assay. The biosensor is first coated with Matrigel, followed by gelation to form 3D matrix. A single spheroid formed using ultralow attachment (ULA) round-bottom microplate is placed on the top surface of the Matrigel. The RWG biosensor is used to monitor the adhesion right after the cells dissociate from the spheroidal structure and invade through the 3D matrix.

EXPERIMENTAL SECTION

Materials. Axitinib was obtained from Selleck Chemicals (Houston, TX, USA). Everolimus, gefitinib, sorafenib, sunitinib, and vandetanib were obtained from LC Laboratories (Woburn, MA, USA). Epidermal growth factor (EGF) was obtained from Bachem (Torrance, CA, USA). Epic 384-well biosensor cell culture compatible microplates, ULA 96-well round bottomed plates, flat bottom 96-well plates, and Corning Matrigel basement membrane matrix 10 mL (Product #354234) were obtained from Corning Incorporated (Corning, NY, USA). Matrigel, once isolated, is approximately 60% laminin, 30% collagen IV, and 8% entactin. Entactin is a bridging molecule that interacts with laminin and collagen IV, and contributes to the structural organization of these ECM molecules. The Matrigel matrix also contains heparan sulfate proteoglycan (perlecan), transforming growth factor-β, EGF, insulin-like growth factor, fibroblast growth factor, tissue plasminogen activator, and other growth factors which occur naturally in the EHS tumor. There is also residual matrix metalloproteinases derived from the tumor cells. Human colorectal adenocarcinoma HT-29 cell line was obtained from American Type Cell Culture (Manassas, VA, USA).

Cell Culture and Spheroid Formation. The HT-29 cells were cultured in the complete medium; that is, McCoy's 5a Medium Modified supplemented with 10% fetal bovine serum, 4.5 g/L glucose, 2 mM glutamine, and 1× Pennstrep at 37 °C under air/5% CO_2. The cells were passed with trypsin/ethylene-diaminetetraacetic acid when approaching 90% confluence to provide new maintenance culture on T-75 flasks and spheroid formation in ULA 96well round bottomed microplates. Spheroids of cells were established by simply dispensing 200 μL cell suspensions at varying seeding densities, 80 000, 40 000, 20 000, 10 000, 5000, 2500, and 1250 cells per well, into the ULA plate. Optimal density for stable spheroid formation was assessed based on the size and shape for each seeding density from day 1 to day 4, as well as the morphology after manually transferred to the biosensor plate using a wide bore pipet tip. The morphology was examined using an inverted light microscope. When needed to maintain spheroids over 4 days, the media was partially exchanged by removing 100 μL old media on day 4 or 7 and then replacing with 100 μL fresh media. All spheroids used were from day 4 to day 8. To safeguard the spheroids from disruption during media changes the pipet tip was held at approximately a 45° angle away from the center of the well bottom.

3D Matrigel Formation. To form 3D gel, Matrigel was first diluted using McCoy's 5a Medium Modified containing 10% FBS, 1× Pennstrep to 0.1 mg/mL (1 × 50 dilution) at 4 °C. Ten microliters of the diluted solution was then added to each well of a 384well biosensor microplate at 4 °C. Afterward, the microplates were incubated inside an incubator at 37 °C under air/5% CO_2 for 24 h to form the 3D gel on the biosensor surface. Matrigel is a liquid at 4 °C and start to form a gel above 10 °C.[16] To prevent premature gelation, Matrigel, the biosensor plates, pipets, and tips all were precooled during the preparation step.

Light Microscopic Imaging. All light microscopic images were collected using Nikon Eclipse TS100 equipped with NIS Elements F3.0 Software (Nikon Instruments Inc., Melville, NY,

dx.doi.org/10.1021/ac502269v | Anal. Chem. 2014, 86, 8842−8849

USA). Data process and analysis were performed using NIH ImageJ (http://imagej.nih.gov/ij/).

DMR Cancer Cell Spheroid Invasion Assays. DMR invasion assays were performed using a high resolution version of Epic BT system (Corning Incorporated).[42,43] This system is a swept wavelength interrogation-based RWG imager which uses a tunable light source to illuminate simultaneously a 3 × 4 biosensor array within a 384-well microplate and a complementary metaloxide semiconductor (CMOS) digital camera to record the resonance images with a spatial resolution of 12 μm. The tunable light source for illumination combines a broadband light source with a high precision, narrow-band optical filter to sweep the wavelength from 823 to 838 nm in a stepwise fashion, each with 100 pm every 20 ms. The resonance image is extracted from 150 spectral images obtained during a single cycle of wavelength sweeping, enabling typical DMR assays with a temporal resolution of 3 s.

The DMR invasion assay includes two steps. First, after gelation the Matrigel coated biosensor plate was washed and incubated with 20 μL the FBS-supplemented media, was then placed onto the imager inside the incubator, and further incubated for approximately 60 min until all biosensors reach a steady baseline. Second, after the baseline was established, the invasion through the 3D Matrigel was initiated by manually placing individual spheroids of HT29 cells in 40 μL of media onto the coated biosensor surface using a wide bore pipet tip. Essential to this step was to ensure the effective pickup of spheroids through visual inspection of pipet tip prior to transfer, to avoid the damage of the Matrigel surface by the tip, and to place appropriately the spheroids within the biosensor area. The DMR signals were continuously monitored for 24 h. To reduce the data point per measurement, the temporal resolution was set at 3 s for first 1 h, 15 s for the next 2 h, and 5 min for the remaining 21 h. For kinase inhibitor studies, the inhibitor at a specific concentration was added into the Matrigel coated biosensor well before spheroid transfer. For EGF studies, the Matrigel was diluted in serum free media to 0.1 mg/mL. After gelation the Matrigel coated plates were washed using the serum-free media, and EGF dissolved in the McCoy media containing 0.1% bovine serum albumin (BSA) was added before assays. The spheroids in ULA plate were also washed carefully with the serum free media. The use of BSA-complemented media is to minimize any potential interference of soluble factors in serum with the effect of EGF on the cancer cell invasion. All DMR assays were performed under physiological conditions.

Statistical Analysis. DMR data were analyzed using GraphPad Prism 5.0 (GraphPad Software Inc., San Diego, CA, USA). The IC_{50} values were obtained by fitting the dose DMR response curves with nonlinear regression. The single cell data was extracted using Corning Epic BT Processor software, and further processed using Microsoft Excel. The inhibitor effect was analyzed using one-way ANOVA Tukey analysis with the Prism 5.0.

RESULTS AND DISCUSSION

Spheroid Formation. We first optimized culture condition in ULA round-bottom 96well plates to form stable and compact spheroids, which is essential to minimize any interference of mechanically dissociated cells from the spheroidal structure with the assay results. HT29 cells were directly seeded onto the ULA plates at varying densities and cultured for up to 4 days, and light microscopic images were collected daily for each density. Results showed that the cells with seeding densities between 20K and 80K per well initially formed irregular aggregates, followed by compaction in size (Figure 2a). After 4

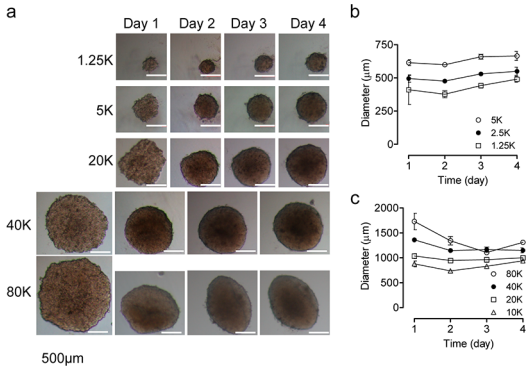

Figure 2. Kinetics and morphology of spheroids formed in ULA round-bottom microplate. (a) Light microscopic imaging reveals the time and cell seeding density dependent formation of 3D spheroids of colon cancer cell line HT29. Scale bar: 500 μm. (b,c) The diameter of spheroids formed using different cell seeding density as a function of culturing time in the microplate. Data represents mean ± s.d. (n = 4).

days culture cells with a seeding density below 40K led to regular spheroidal structure, while cells with a seeding density of 80K resulted in an elongated spheroidal structure. Interestingly, after 4 days culture cells with a seeding density below 10K formed transitional spheroids; that is, these spheroids continued growing in size over 4 days (Figure 2b). In contrast, cells with a seeding density above 10K resulted in apparently stable spheroids (Figure 2c). The mechanical stability of spheroids formed after 4 days was further examined by manually transferring to a 96well flat bottom or 384well biosensor microplate, both coated with Matrigel, using wide-bore pipet tips. Light microscopic imaging showed that only spheroids obtained using cells with a seeding density of 20K or 40K remain intact right after transferring, as evidenced by the absence of individual cells or small cell clusters, beside the spheroids (exemplified in Figure 3). These results suggest that combining ultralow attachment surface chemistry with round-bottom geometry is effective to promote the formation of HT29 spheroids, consistent with previous reports.[56] These results also suggest that the optimal seeding density is between 20K and 40K per well for the formation of stable HT29 spheroids. Therefore, we next focused on investigating the invasive behavior of spheroids formed using a seeding density of 40K.

RWG Imaging of the Invasion of Cells in Spheroid through Matrigel. We hypothesized that the RWG biosensor can monitor in real-time the adhesion of cancer cells as a result of the invasion through 3D Matrigel, and the DMR profiles can be used as an indicator to determine the invasion process. To validate this hypothesis, we compared the characteristics of DMR responses of a single HT29 spheroid after placed onto a biosensor surface with and without Matrigel coating. The DMR on the uncoated surface is arising from the adhesion after the cells dissociate from the spheroidal structure; however, the DMR on the coated surface is a result of adhesion after the cells dissociate from the spheroid and invade through the Matrigel.

First, we compared the DMR images of a single HT29 spheroid on a biosensor surface with and without Matrigel coating. The time series DMR images were obtained after the

dx.doi.org/10.1021/ac502269v | Anal. Chem. 2014, 86, 8842−8849

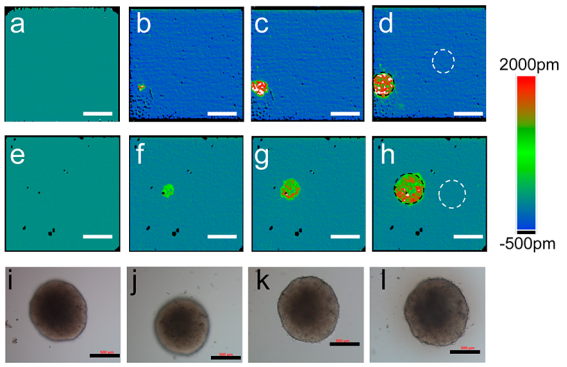

Figure 3. Representative DMR images of the invasion and adhesion of cells from a single spheroid. (a–d) The time series DMR images of a single spheroid before and after placing onto an uncoated biosensor surface: 0 min (a), 1 h (b), 6 h (c), and 24 h (d). (e–h) The time series DMR images of a single spheroid before and after placing onto a biosensor surface coated with 10 μL of 0.1 mg/mL Matrigel: 0 min (e), 1 h (f), 6 h (g), and 24 h (h). Spatial scale bar: 500 μm. Intensity scale bar: false colored (−500 pm to 2000 pm). (i–l) The time series light microscopic images of a single spheroid before and after placing onto Matrigel coated biosensor surface: 0 min (e), 1 h (f), 6 h (g), and 24 h (h). Scale bar: 500 μm. Condition of spheroid formation: 40K per well seeding density, 4 days culture.

starting resonant wavelength at all pixels was normalized to zero (Figure 3a and e). Results showed that the contact of a spheroid with the uncoated surface over 24 h led to a time-dependent and continuous expansion of a circular area having positive DMR signals (Figure 3b–d). Similar behavior was observed on the coated biosensor (Figure 3e–h). Light microscopic imaging showed that during 24 h assay period the spheroidal structure remains to be intact on the coated surface (Figure 3i–l), as well as the uncoated surface (data not shown). The starting spheroids were almost identical in diameter, 1145 and 1123 μm on the coated and uncoated surfaces, respectively. However, compared to the uncoated surface the DMR signal intensity was smaller and the area having positive DMR signals are greater on the coated surface (comparing Figure 3h with Figure 3d), the latter of which may be due to the presence of growth factors in Matrigel. Some of these growth factors seem promote cell migration and invasion (see below). Of note, for the coating achieved through gelation of 10 μL of Matrigel solution we estimated the height of 3D matrix to be 630 μm, given that the well diameter is 4.5 mm and the coating is assumed to be uniform.

Second, we examined the characteristics of DMR signals at the single pixel/single cell level. To perform single cell analysis we first estimated the initial adhesion point by identifying the pixelated location at which a positive DMR first occurred. The initial adhesion point is the location at which the first single cell adheres onto the sensor surface. For spheroids on the 3D matrix the initial adhesion point also approximates very closely to the initial contact point of the spheroid with the 3D matrix, at which the cell has the shortest distance to invade through the matrix. Next, we designed the coordinate of the initial adhesion point as (0,0), and then calculated the lateral distances of all pixels of the biosensor from it. For a spheroid on the uncoated surface, this distance approximates very closely to the travel distance of a cell. However, for a spheroid on the 3D Matrigel this distance is not the travel distance of an invading cell; instead, it represents the distance of the cell relative to the location at which the first single cell invades through the 3D Matrigel, arrives and adheres onto the sensor surface. Tumor cells are known to invade through the 3D ECM via both matrix metalloproteinase (MMP)-independent and dependent mechanisms, and the overall invasion is dependent on the interplay between the two mechanisms.[57,58] The MMP-independent invasion is sensitive to the pore size of the 3D matrix and the deformability of the cell nucleus, while the MMP-dependent

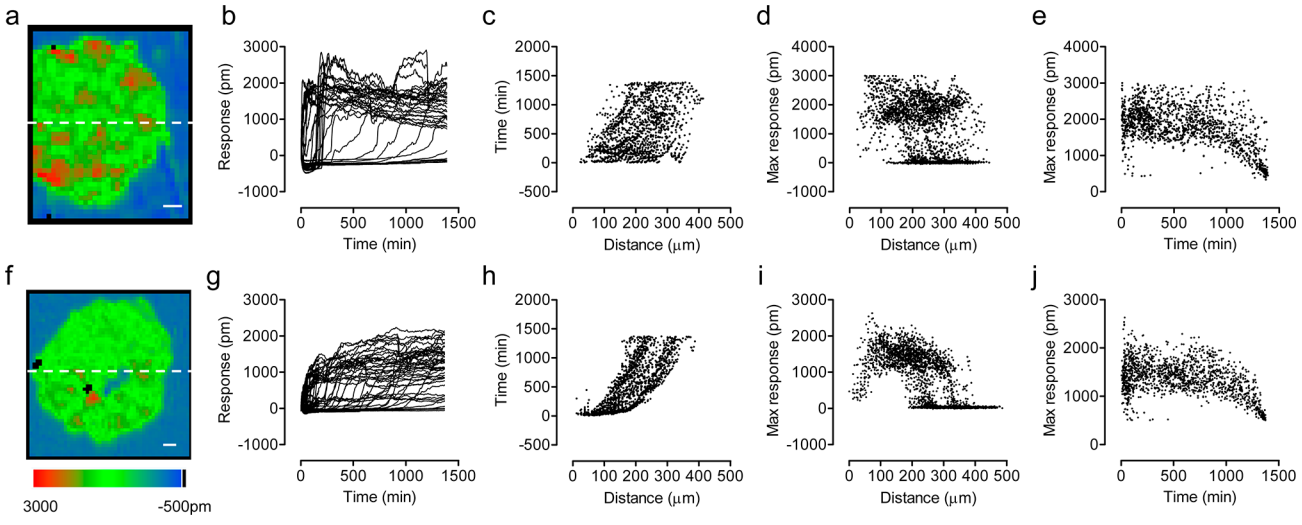

Figure 4. Single pixel analysis of the DMR signals after placing a spheroidal cell culture on a biosensor. (a–e) The DMR characteristics of a spheroid on the uncoated surface: (a) DMR image taken 24 h after the spheroid positioning, scale bar is 50 μm; (b) pixelated real-time DMR signals for the line indicated in (a); (c) the correlation between the adhesion time and the distance relative to the first contact point; (d) the correlation between the maximal response and the relative distance; (e) the correlation between the adhesion time and the maximal response. (f–j) The DMR characteristics of a spheroid on the Matrigel: (f) DMR image taken 24 h after the spheroid positioning, scale bar is 50 μm; (g) pixelated real-time DMR signals for the line indicated in (f); (h) the correlation between the adhesion time and the distance relative to the first adhesion point; (i) the correlation between the maximal response and the relative distance; (j) the correlation between the adhesion time and the maximal response. For f–j, the 3D matrix coating was achieved using 10 μL of 0.1 mg/mL Matrigel. Condition of spheroid formation: 40K per well seeding density, 4 days culture.

dx.doi.org/10.1021/ac502269v | *Anal. Chem.* 2014, 86, 8842–8849

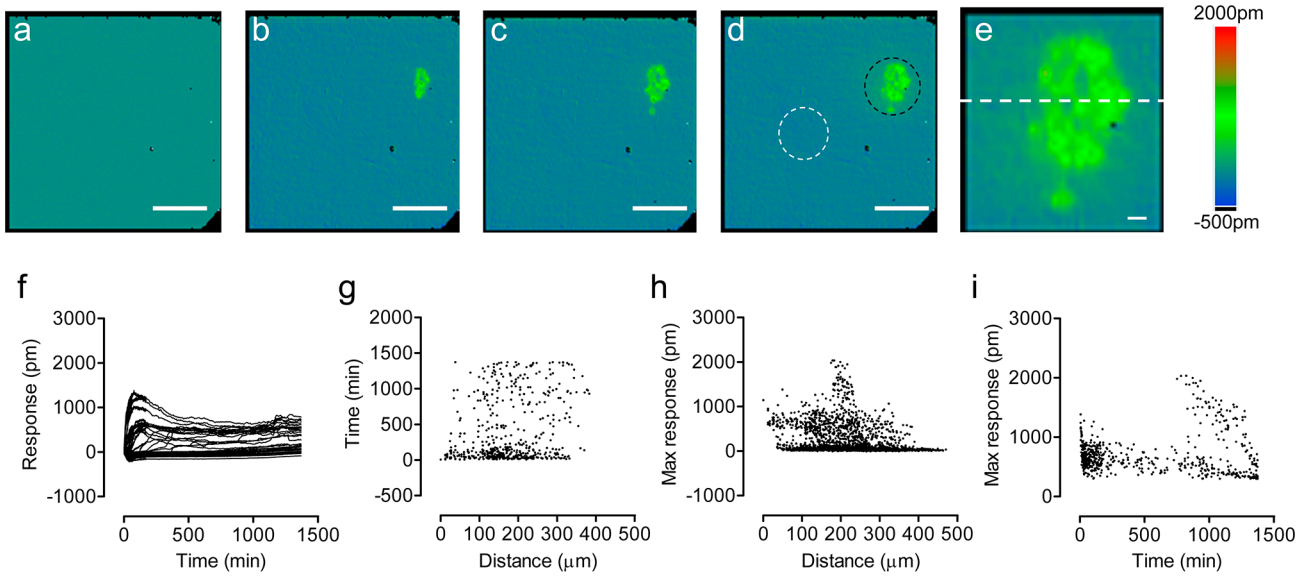

Figure 5. Single pixel analysis of the DMR signals arising from the invasion and adhesion of cells on the Matrigel in the presence of vandetanib. (a–e) DMR images taken at different time: 0 min (a), 1 h (b), 6 h (c) and 24 h (d). (e) is the zooming image of (d). Scale bar is 500 μm for a–d and 50 μm for e. (f) Pixelated real-time DMR signals for the line indicated in (e); (g) the correlation between the adhesion time and the distance relative to the first adhesion point; (h) the correlation between the maximal response and the relative distance; (i) the correlation between the adhesion time and the maximal response. The 3D matrix coating was achieved using 10 μL 0.1 mg/mL Matrigel. Condition of spheroid formation: 40K per well seeding density, 4 days culture.

invasion uses active invadopodia containing the cell surface MMPs to degrade the ECM and enlarge matrix pore diameters.[58] Although it is obviously difficult to separate the contributions of the two distinct mechanisms to the overall invasion, the MMP-independent mechanism was found to the main contributor to cell invasion in the low density 3D gel.[58] We here used low concentration of Matrigel (0.1 mg/mL). Furthermore, for spheroids on the 3D Matrigel the DMR is resulted from the cell adhesion after invasion through the 3D matrix. Given that all cells need invade the same 3D matrix, we reasoned that the lateral distance is a useful parameter to investigate the invasion behavior of spheroidal cells. Finally, we calculated the maximal response and the adhesion time required to reach a positive DMR amplitude of 500 pm for each location. The maximal response of the DMR obtained reflects the degree of cell adhesion. Given that the kinetics of cell adhesion is relatively rapid (see below), the adhesion time obtained mostly reflect the time required for a cell to invade through the matrix and arrive at the sensor surface.

Results showed that on the uncoated surface the pixelated DMR gave rise to location-dependent kinetic profiles (Figure 4a–e). The earlier the DMR occurs, the faster the kinetics is to reach its maxima (Figure 4b). For all locations none of these positive DMR, when occurring, was found to decay back to the baseline, suggesting no or little cell movement after attachment. Correlation analysis showed that there is a poor or little correlation between the relative distance and the cell adhesion time (Figure 4c). The maximal response was also poorly correlated with the distance relative to the initial contact point, and there was little or no DMR outside the cell adhesion area (Figure 4d). The maximal response was smaller when the adhesion occurs at the time approaching the end point of the assay (24 h), reflecting the incomplete adhesion (Figure 4e). These results are better explained by which on the uncoated surface the cells dissociate from the spheroidal structure, migrate toward and adhere onto specific locations of the sensor surface.

For the coated surface the spheroid also gave rise to location-dependent DMR signals, but with different features (Figure 4f–j). First, the duration for a DMR event from starting to completion is generally longer, compared to the DMR event occurring at corresponding time point on the uncoated surface (comparing Figure 4g with Figure 4b). Second, there is a clear correlation between the relative distance and the adhesion time (Figure 4h). As the relative distance increases, the adhesion time increases, suggesting that the 3D matrix acts as a microenvironment barrier to govern the invasion and adhesion path. Interestingly, it appears to have two distinct populations of cells displaying distinct invasion and adhesion kinetics, the origin of which is unknown and worthy of further mechanistic studies. Third, compared to those on the uncoated surface, the maximal response is much smaller and more sensitive to the location relative to the initial adhesion point (Figure 4i). The maximal responses at the pixels near the contact point are relatively small, possibly due to the suppression of the soft matrix by the spheroid which makes the invasion and adhesion difficult. In contrast, the maximal responses at the pixels away from the contact point are quite uniform and comparably greater, although when approaching the border of invasion and adhesion area the maximal responses progressively decrease again mostly because of incomplete adhesion. Fourth, compared to the uncoated surface the maximal responses occurring at corresponding time point were generally smaller (Figure 4j). The migrating cells are believed to preferably take the route of least resistance.[24] However, it is more likely that once dissociated from the spheroid some cells may first travel along the surface of the gel, then invade through the 3D matrix and finally adhere onto the biosensor surface, while other cells may directly invade through the gel to reach the adhesion sites. The two possible routes may be accounted for the two populations of cells observed (Figure 4h). Fifth, the time

dx.doi.org/10.1021/ac502269v | Anal. Chem. 2014, 86, 8842–8849

required for the first DMR event to occur was 5.2 ± 0.4 min (n=3) on the 3D Matrigel, relatively slower than that on the uncoated surfaces (2.5 ± 0.3 min, n = 3). This difference suggests that the minimal time to invade through the 3D gel is between 2.7 and 5.2 min. The rapid invasion observed here may be due to multiple factors, including the use of low density 3D gel (0.1 mg/mL Matrigel), the presence of chemoattractants in the Matrigel, and the DMR single cell measurement of early invasion events. Previous microscopy imaging of the late stage invasion of cancer cell spheroids showed that the velocity of cancer cell invasion was in the range of several μm/h in the dense ECM gels and increased significantly in the presence of chemoattractants;[59] however, the cell invasion velocity could be as high as 10−20 μm/min in low density gels made of 0.3 mg/mL rat tail collagen.[58] Of not, these studies were based on the invasive behavior of a population of cells. A recent study at subcellular level showed that active invadopodia can effectively degrade the ECM within several minutes.[60] The ECM degradation at invadopodia provides room for initial protusions and rapidly increases the pore size of the 3D gel, enabling rapid cell invasion. Given that there are greater numbers of cells available to ECM binding and invadopodia formation at the initial contact area of the spheroid with the 3D Matrigel, the ECM degradation and cell invasion could be much faster than these locations far away from the initial contact area. This is indeed consistent with the apparently exponential increase of the invasion/adhesion time as the distance from the initial adhesion point increases (Figure 4h). Our rapid invasion results seem reasonably consistent with the kinetics of ECM degradation by active invadopodia. Lastly, the total number of cell adhesion events is much higher on the coated surface than that on the uncoated surface. In fact, 24 h after the spheroid was placed there were 897 and 1492 pixels whose DMR were greater than 500 pm on the uncoated and coated surfaces, respectively, suggesting that the Matrigel promotes cell invasion, thus increasing the number of cell adhesion events. Nonetheless, these results are better explained by which on Matrigel the cells can indeed dissociate from the spheroidal structure, invade through the 3D matrix, migrate toward and adhere onto the sensor surface.

Molecular Profiling of Kinase Inhibitors to Alter the Invasion and Adhesion Process. Next, we examined the effect of vandetanib on the invasion and adhesion process of spheroidal cell clusters. Vandetanib is a multikinase inhibitor for a multitude of tyrosine kinases including EGF receptors (EGFR), vascular endothelial growth factor receptor (VEGFR), and c-Met receptor.[61,62] DMR imaging showed that the presence of vandetanib significantly suppressed the invasion and adhesion process (Figure 5a-e). Several interesting features occur. First, the DMR amplitudes were generally much smaller than those in the absence of vandetanib (comparing Figure 5f with Figure 4g), suggesting that vandetanib has an inhibitory effect on cell adhesion. Second, vandetanib also reduced significantly the total number of invasion/adhesion events. 24 h after the spheroid was placed there were 1492 pixels whose DMR were greater than 500 pm on the 3D gel surface. In contrast, the presence of 16 μM vandetanib reduced the number of pixels with a DMR greater than 500 pm to 351, and 71% of which occurred within the first 2 h. These results suggest that vandetanib is also effective to prevent cell invasion, in particular later cell invasion. Third, vandetanib had little effect on the time required for the first DMR event to occur. This time was found to be 5.4 ± 0.3 min (n=3) for the spheroids on the 3D matrix in the presence of vandetanib. Fourth, unlike that in the absence of vandetanib, there was a poor correlation between the relative distance and the invasion and adhesion time (Figure 5g). The maximal response was also poorly correlated with the relative distance (Figure 5h). Fifth, the most notable was that only small portion of invasion events led to a DMR event similar to those in the absence of vandetanib, but occurred toward the end of assay (Figure 5i). These results are best explained by that vandetanib suppresses the invasion through the 3D matrix, and only small numbers of cells escape the inhibition so they can invade through the 3D matrix and adhere onto the sensor surface. These results also provide evidence supporting that the DMR is a result of cell adhesion after invasion through the 3D gel, rather than the contact with the top surface of the 3D gel.

Finally, we examined the effect of a panel of kinase inhibitors and EGF on the invasion and adhesion process, based on the average responses induced by spheroids. Sunitinib is an inhibitor of VEGFR2, PDGFR, and KIT;[63] sorafenib is an inhibitor of VEGFR2, PDGFR, c-Raf, and B-Raf;[64] gefitinib is an EGFR inhibitor;[65,66] everolimus is an mTOR inhibitor;[67] axitinib is an inhibitor of VEGFR1-3, c-KIT, and PDGFR.[68] Given that the biosensor dimension is much greater than the adhesion area of cells from the spheroidal structure, an intrasensor self-referencing can be used to filter out nonspecific signal arising from potential mismatch in temperature or bulk index, or other operational interference (Figure 6a−c). Results showed that the spheroid gave rise to greater and faster averaged DMR on the uncoated surface than the coated surface (comparing Figure 6a with Figure 6b). Vandetanib at 16 μM almost completely suppressed the DMR (Figure 6c), and its inhibitory effect was found to be dose-dependent, yielding an apparent $\log EC_{50}$ of −5.36 ± 0.06 (n = 3) (Figure 6d). Similarly, sunitinib, sorafenib and gefitinib at 16 μM all significantly suppressed the invasion and adhesion DMR of spheroids (p < 0.05), but everolimus and axitinib had little effects (Figure 6e). The different inhibitory effects of these kinase inhibitors on the invasion of 3D cells through the 3D matrix observed reflect the complex pharmacology arising from their polypharmacology, phenotypic pharmacology and on-target pharmacology.[54] In contrast, EGF gave rise to a bell-shaped dose response to accelerate the invasion and adhesion DMR of spheroids; and the maximal stimulatory effect was observed at 100 nM EGF (Figure 6f), consistent with previous reports.[69] Nonetheless, these results suggest that the DMR-based assay is effective to study cancer cell invasion through the 3D matrix.

■ CONCLUSION

Motility and invasion are key hallmarks distinguishing benign from malignant tumors, offering a rich source of novel molecular targets for developing inhibitors to restrain both metastasis and angiogenesis. 3D cancer cell models are increasingly recognized to be important for anticancer drug discovery due to their ability to recapitulate the in vivo properties of solid tumors.[70] However, current assays to quantitatively measure cell movement and invasion, in particular in 3D matrix, are cumbersome. Here we demonstrated a label-free, real-time, single-cell and quantitative assay to measure the invasion of 3D cell spheroids through the 3D Matrigel. This is possible by using three distinct techniques: (i) ultralow attachment surface in conjunction with round-bottom geometry was used to generate mechanically stable cancer cell

dx.doi.org/10.1021/ac502269v | Anal. Chem. 2014, 86, 8842−8849

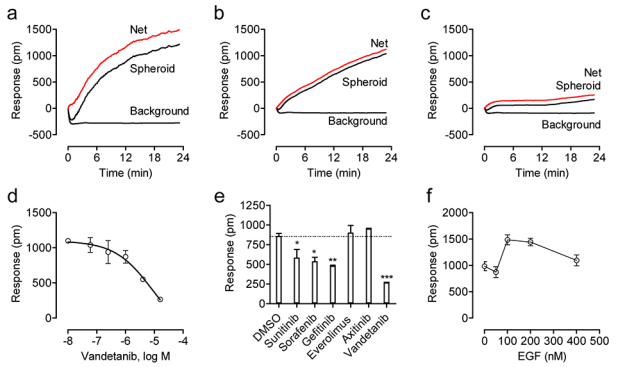

Figure 6. Characteristics of the population averaged DMR arising from the adhesion of cells onto the biosensor surface. (a–c) Real-time population averaged DMR under different conditions: (a) uncoated biosensor surface; (b) Matrigel coated surface in the absence of vandetanib; (c) Matrigel coated surface in the presence of 16 μM vandetanib. The average DMR was obtained from the maximal contact area of the spheroid after 24 h assay (indicated by the black broken circle), where the background signal was obtained from the area outside the spheroid (indicated by the white broken circle in Figure 3d for a, Figure 3h for b, and Figure 5d for c). The background signal can be filtered out using the intrasensor reference so the true response (net) can be calculated. (d) The dose inhibition response of vandetanib. (e) The selective inhibition of different kinase inhibitors. *$p < 0.05$; **$p < 0.001$; ***$p < 0.0001$. (f) The DMR response 24 h post invasion and adhesion as a function of EGF doses. For d–f, the average DMR amplitudes at 24 h post stimulation were plotted. For d and e, the contact area of the spheroid at 24 h post stimulation was used as the reference for comparative analysis, while for f, the contact area of the spheroid in the presence of 100 nM EGF at 24 h post stimulation was used the reference. Data in d, e, and f represent mean ± s.d. ($n = 3$). For d–f, the net responses were analyzed. Condition of spheroid formation: 40K per well seeding density, 4 days culture for the control, vandetanib and sorafenib, or 5 days culture for EGF, everolimus, gefitinib, axitinib, and sunitinib.

spheroids with high reproducibility and simplicity; (ii) the spontaneous gelation of Matrigel under physiological condition was used to form 3D Matrigel; and (iii) spatially resolved RWG imager was used to record DMR images and extract DMR signals arising from the adhesion after cells dissociate from the spheroid and invade through the 3D matrix. Results showed that the RWG imager can detect the invasion and adhesion process of multicellular spheroids, EGF promotes the invasion, but several kinase inhibitors including vandetanib, gefitinib, and sorafenib inhibit the invasion.

The biosensor-based invasion assay is advantageous in several aspects. First, this assay is noninvasive and does not require any labels, so it bypasses cell manipulation steps, such as staining or cell transfection, or pre- and postexperimental processing steps that are common to most of conventional assays.[24] Second, this assay offers real-time kinetic measurements, unlike most of conventional assays which only provide end point results.[12] Third, this assay can detect early cell invasion process of spheroidal cells through 3D matrix. This is almost impossible using real-time light microscopy imaging, which is limited to detect cells invading out of the outer border of spheroids placed in the 3D matrix gel.[40,41] The present invasion assay is quantitative and useful for studying the invasion mechanisms at single cell level and for screening drug molecules that interfere with the invasion process. The recently developed whole plate RWG imager,[71] although with relatively low spatial resolution (~80 μm), may be useful to screen and identify novel antiangiogenesis inhibitors with moderate and high throughput, when the end point measurement is used. Alternatively, mid-infrared surface plasmon resonance with long sensing depth[72] may be able to monitor both invasion and adhesion processes. It is worthy of noting that total internal reflection fluorescence (TIRF) imaging can also be used to study the invasion of spheroidal cells through 3D matrix, given that it selectively excites fluorophores within its evanescent wave. Recently, we had found that the TIRF measurements led to kinetic responses similar to the DMR measurements for several receptors.[73] Of note, given the current biosensor design (2 × 2 mm biosensor in each well), care is warranted to ensure appropriate positioning of a single spheroid onto each sensor. Increasing the sensor dimension or adding two spheroids into each well are two possible means to achieve appropriate positioning. In addition, care must be taken to interpret the data, since the biosensor has short penetration depth and detects the adhesion event after invasion through the 3D matrix. The true distance that the invading cells traveled are unknown, neither are the history of adjacent cells, so it is difficult to separate collective invasion from individual ones. Nevertheless, we here demonstrate the ability of spatially resolved RWG imager for label-free, real-time, single-cell and quantitative monitoring of the invasion of 3D cancer cells through 3D matrix and its subsequent adhesion on the biosensor surface.

AUTHOR INFORMATION

Corresponding Author

*E-mail: fangy2@corning.com.

Present Address

†N.K.F.: Department of Biomedical Engineering, University of South Florida, Tampa, Florida.

Author Contributions

N.K.F. and A.M.F. designed and performed experiments and analyzed the data. Y.F. conceived the idea, designed the experiments, analyzed all data, and wrote the manuscript. All authors have given approval to the final version of the manuscript.

Notes

The authors declare the following competing financial interest(s): Y.F. and A.M.F are employees and stockholders of Corning Incorporated. Epic systems, Matrigel, and ULA round-bottom microplates are commercial products from Corning. DMR assays are patented by Corning.

REFERENCES

(1) Hanahan, D.; Weinberg, R. A. *Cell* **2011**, *144*, 646–674.
(2) Valastyan, S.; Weinberg, R. A. *Cell* **2011**, *147*, 275–292.
(3) Klein, C. A. *Nature* **2013**, *501*, 365–372.
(4) Friedl, P.; Wolf, K. *Nat. Rev. Cancer* **2003**, *3*, 362–374.
(5) Friedl, P.; Alexander, S. *Cell* **2011**, *147*, 992–1009.
(6) Friedl, P.; Locker, J.; Sahai, E.; Segall, J. E. *Nat. Cell Biol.* **2012**, *14*, 777–783.
(7) Stetler-Stevenson, W. G.; Aznavoorian, S.; Liotta, L. A. *Annu. Rev. Cell Biol.* **1993**, *9*, 541–573.
(8) Poincloux, R.; Lizárraga, F.; Chavrier, P. *J. Cell. Sci.* **2009**, *122*, 3015–3024.
(9) Desgrosellier, J. S.; Cheresh, D. A. *Nat. Rev. Cancer* **2010**, *10*, 9–22.
(10) Steeg, P. S.; Theodorescu, D. *Nat. Clin. Pract. Oncol.* **2008**, *5*, 206–219.
(11) Eccles, S. A.; Box, C.; Court, W. *Biotechnol. Annu. Rev.* **2005**, *11*, 391–421.

(12) Albini, A.; Benelli, R. *Nat. Protoc.* **2007**, *2*, 504−511.
(13) Kam, Y.; Guess, C.; Estrada, L.; Weidow, B.; Quaranta, V. *BMC Cancer* **2008**, *8*, 198.
(14) Carragher, N. *Clin. Exp. Metast.* **2009**, *26*, 381−397.
(15) Kleinman, H. K.; Martin, G. R. *Semin. Cancer Biol.* **2005**, *15*, 378−386.
(16) Benton, G.; Kleinman, H. K.; George, J.; Arnaoutova, I. *Int. J. Cancer* **2011**, *128*, 1751−1757.
(17) Quail, D. F.; Maciel, T. J.; Rogers, K.; Postovit, L. M. *J. Biomol. Screen.* **2012**, *17*, 1088−1095.
(18) Fisher, K. E.; Pop, A.; Koh, W.; Anthis, N. J.; Saunders, W. B.; Davis, G. E. *Mol. Cancer.* **2006**, *5*, 69.
(19) Brekhman, V.; Neufeld, G. *BMC Cancer* **2009**, *9*, 415−427.
(20) Pathak, A.; Kumar, S. *Integr. Biol.* **2011**, *3*, 267−278.
(21) Koch, T. M.; Münster, S.; Bonakdar, N.; Butler, J. P.; Fabry, B. *PLoS One* **2012**, *7*, e33476.
(22) Cheung, K. J.; Gabrielson, E.; Werb, Z.; Ewald, A. J. *Cell* **2013**, *155*, 1639−1651.
(23) Liu, L.; Duclos, G.; Sun, B.; Lee, J.; Wu, A.; Kam, Y.; Sontag, E. D.; Stone, H. A.; Sturm, J. C.; Gatenby, R. A.; Austin, R. H. *Proc. Natl. Acad. Sci. U.S.A.* **2013**, *110*, 1686−1691.
(24) Kramer, N.; Walzl, A.; Unger, C.; Rosner, M.; Krupitza, G.; Hengstschläger, M.; Dolznig, H. *Mutat. Res.* **2013**, *752*, 10−24.
(25) Justice, B. A.; Badr, N. A.; Felder, R. A. *Drug Discovery Today* **2009**, *14*, 102−107.
(26) Wolf, K.; Wu, Y. I.; Liu, Y.; Geiger, J.; Tam, E.; Overall, C.; Stack, M. S.; Friedl, P. *Nat. Cell Biol.* **2007**, *9*, 893−904.
(27) Hait, W. N. *Nat. Rev. Drug Discovery* **2010**, *9*, 253−254.
(28) Hutchinson, L.; Kirk, R. *Nat. Rev. Clin. Oncol.* **2011**, *8*, 189−190.
(29) Chitcholtan, K.; Asselin, E.; Parent, S.; Sykes, P. H.; Evans, J. J. *Exp. Cell Res.* **2013**, *319*, 75−87.
(30) Härmä, V.; Virtanen, J.; Mäkelä, R.; Happonen, A.; Mpindi, J. P.; Knuuttila, M.; Kohonen, P.; Lötjönen, J.; Kallioniemi, O.; Nees, M. *PLoS One* **2010**, *5*, e10431.
(31) Pickl, M.; Ries, C. H. *Oncogene* **2009**, *28*, 461−468.
(32) Luca, A. C.; Mersch, S.; Deenen, R.; Schmidt, S.; Messner, I.; Schäfer, K. L.; Baldus, S. E.; Huckenbeck, W.; Piekorz, R. P.; Knoefel, W. T.; Krieg, A.; Stoecklein, N. H. *PLoS One* **2013**, *8*, e59689.
(33) Lawrenson, K.; Sproul, D.; Grun, B.; Notaridou, M.; Benjamin, E.; Jacobs, I. J.; Dafou, D.; Sims, A. H.; Gayther, S. A. *Carcinogenesis* **2011**, *32*, 1540−1549.
(34) Busse, A.; Letsch, A.; Fusi, A.; Nonnenmacher, A.; Stather, D.; Ochsenreither, S.; Regenbrecht, C. R.; Keilholz, U. *Clin. Exp. Metastasis* **2013**, *30*, 781−791.
(35) Tibbitt, M. W.; Anseth, K. S. *Sci. Transl. Med.* **2012**, *4*, 160ps124.
(36) Nummer, D.; Suri-Payer, E.; Schmitz-Winnenthal, H.; Bonertz, A.; Galindo, L.; Antolovich, D.; Koch, M.; Buchler, M.; Weitz, J.; Schirrmacher, V.; Beckhove, P. *J. Natl. Cancer Inst.* **2007**, *99*, 1188−1199.
(37) Ghosh, S.; Joshi, M. B.; Ivanov, D.; Feder-Mengus, C.; Spagnoli, G. C.; Martin, I.; Erne, P.; Resink, T. J. *FEBS Lett.* **2007**, *581*, 4523−4528.
(38) Oxmann, D.; Held-Feindt, J.; Stark, A. M.; Hattermann, K.; Yoneda, T.; Mentlein, R. *Oncogene* **2008**, *27*, 3567−3575.
(39) Sabeh, F.; Shimizu-Hirota, R.; Weiss, S. J. *J. Cell Biol.* **2009**, *185*, 11−19.
(40) Korff, T.; Augustin, H. G. *J. Cell Sci.* **1999**, *112*, 3249−3258.
(41) Kniazeva, E.; Putnam, A. J. *Am. J. Physiol. Cell Physiol.* **2009**, *297*, C179−C187.
(42) Ferrie, A. M.; Deichmann, O. D.; Wu, Q.; Fang, Y. *Appl. Phys. Lett.* **2012**, *100*, No. 223701.
(43) Ferrie, A. M.; Wu, Q.; Deichmann, O.; Fang, Y. *Appl. Phys. Lett.* **2014**, *104*, No. 183702.
(44) Fang, Y.; Ferrie, A. M.; Fontaine, N. H.; Mauro, J.; Balakrishnan, J. *Biophys. J.* **2006**, *91*, 1925−1940.
(45) Fang, Y.; Ferrie, A. M.; Fontaine, N. H.; Yuen, P. K. *Anal. Chem.* **2005**, *77*, 5720−5725.
(46) Schroder, R.; Janssen, N.; Schmidt, J.; Kebig, A.; Merten, N.; Hennen, S.; Müller, A.; Blättermann, S.; Mohr-Andrä, M.; Zahn, S.; Wenzel, J.; Smith, N. J.; Gomeza, J.; Drewke, C.; Milligan, G.; Mohr, K.; Kostenis, E. *Nat. Biotechnol.* **2010**, *28*, 943−949.
(47) Verrier, F.; An, S.; Ferrie, A. M.; Sun, H.; Kyoung, M.; Fang, Y.; Benkovic, S. J. *Nat. Chem. Biol.* **2011**, *7*, 909−915.
(48) Fang, Y. *Drug Discovery Today Technol.* **2010**, *7*, e5−e11.
(49) Ferrie, A. M.; Wang, C.; Deng, H.; Fang, Y. *Integr. Biol.* **2013**, *5*, 1253−1261.
(50) Fang, Y.; Ferrie, A. M. *FEBS Lett.* **2008**, *582*, 558−564.
(51) Goral, V.; Jin, Y.; Sun, H.; Ferrie, A. M.; Wu, Q.; Fang, Y. *PLoS One* **2011**, *6*, e19282.
(52) Ferrie, A. M.; Sun, H.; Fang, Y. *Sci. Rep.* **2011**, *1*, 33.
(53) Deng, H.; Wang, C.; Su, M.; Fang, Y. *Anal. Chem.* **2012**, *84*, 8232−8239.
(54) Fang, Y. *J. Pharmacol. Tox. Methods* **2013**, *67*, 69−81.
(55) Fang, Y. *Front. Pharmacol.* **2014**, *5*, 52.
(56) Vinci, M.; Gowan, S.; Boxall, F.; Patterson, L.; Patterson, L.; Zimmermann, M.; Court, W.; Lomas, C.; Mendiola, M.; Hardisson, D.; Eccles, S. A. *BMC Biol.* **2012**, *10*, 29.
(57) Wang, Y.; McNiven, M. A. *J. Cell Biol.* **2012**, *196*, 375−385.
(58) Wolf, K.; Te Lindert, M.; Krause, M.; Alexander, S.; Te Riet, J.; Willis, A. L.; Hoffman, R. M.; Figdor, C. G.; Weiss, S. J.; Friedl, P. *J. Cell Biol.* **2013**, *201*, 1069−1084.
(59) Deisboeck, T. S.; Berens, M. E.; Kansal, A. R.; Torquato, S.; Stemmer-Rachamimov, A. O.; Chiocca, E. A. *Cell Prolif.* **2001**, *34*, 115−134.
(60) Hoshino, D.; Koshikawa, N.; Suzuki, T.; Quaranta, V.; Weaver, A. M.; Seiki, M.; Ichikawa, K. *PLoS Comput. Biol.* **2012**, *8*, e1002479.
(61) Carlomagno, F.; Vitagliano, D.; Guida, T.; Ciardiello, F.; Tortora, G.; Vecchio, G.; Ryan, A. J.; Fontanini, G.; Fusco, A.; Santoro, M. *Cancer Res.* **2002**, *62*, 7284−7290.
(62) Wedge, S. R.; Ogilvie, D. J.; Dukes, M.; Kendrew, J.; Chester, R.; Jackson, J. A.; Boffey, S. J.; Valentine, P. J.; Curwen, J. O.; Musgrove, H. L.; Graham, G. A.; Hughes, G. D.; Thomas, A. P.; Stokes, E. S.; Curry, B.; Richmond, G. H.; Wadsworth, P. F.; Bigley, A. L.; Hennequin, L. F. *Cancer Res.* **2002**, *62*, 4645−4655.
(63) Pàez-Ribes, M.; Allen, E.; Hudock, J.; Takeda, T.; Okuyama, H.; Viñals, F.; Inoue, M.; Bergers, G.; Hanahan, D.; Casanovas, O. *Cancer Cell* **2009**, *15*, 220−231.
(64) Wilhelm, S. M.; Adnane, L.; Newell, P.; Villanueva, A.; Llovet, J. M.; Lynch, M. *Mol. Cancer Ther.* **2008**, *7*, 3129−3140.
(65) Sordella, R.; Bell, D. W.; Haber, D. A.; Settleman, J. *Science* **2004**, *305*, 1163−1167.
(66) Knight, Z. A.; Lin, H.; Shokat, K. M. *Nat. Rev. Cancer* **2010**, *10*, 130−137.
(67) Abraham, R. T. *Curr. Opin. Immunol.* **1998**, *10*, 330−336.
(68) Escudier, B.; Gore, M. *Drugs Res. Dev.* **2011**, *11*, 113−126.
(69) Kim, H. D.; Guo, T. W.; Wu, A. P.; Wells, A.; Gertler, F. B.; Lauffenburger, D. A. *Mol. Biol. Cell* **2008**, *19*, 4249−4259.
(70) Kunz-Schughart, L. A.; Freyer, J. P.; Hofstaedter, F.; Ebner, R. *J. Biomol. Screen.* **2004**, *9*, 273−285.
(71) Ferrie, A. M.; Wu, Q.; Fang, Y. *Appl. Phys. Lett.* **2010**, *97*, No. 223704.
(72) Yashunsky, V.; Shimron, S.; Lirtsman, V.; Weiss, A. M.; Melamed-Book, N.; Golosovsky, M.; Davidov, D.; Aroeti, B. *Biophys. J.* **2009**, *97*, 1003−1012.
(73) Chen, M.; Zaytseva, N. V.; Wu, Q.; Li, M.; Fang, Y. *Appl. Phys. Lett.* **2013**, *102*, No. 193702.